Electronic Supplementary Material (ESI) for Physical Chemistry Chemical Physics.
This journal is © the Owner Societies 2018

Electronic Supplementary Information

Understanding the roles of plasmonic Au nanocrystal size, shape, aspect ratio and loading amount in Au/g-C_3N_4 hybrid nanostructures for photocatalytic hydrogen generation

Yanzhen Guo,[a] Henglei Jia,[b] Jianhua Yang,[b] Hang Yin,[b] Zhi Yang,*[a] Jianfang Wang*[b] and Baocheng Yang[c]

[a]Key Laboratory for Thin Film and Microfabrication of Ministry of Education, Department of Micro/Nano Electronics, School of Electronic Information and Electrical Engineering, Shanghai Jiao Tong University, Shanghai 200240, China

[b]Department of Physics, The Chinese University of Hong Kong, Shatin, Hong Kong SAR, China

[c]Henan Provincial Key Laboratory of Nanocomposites and Applications, Institute of Nanostructured Functional Materials, Huanghe Science and Technology College, Zhengzhou 450006, China

Supplementary figures

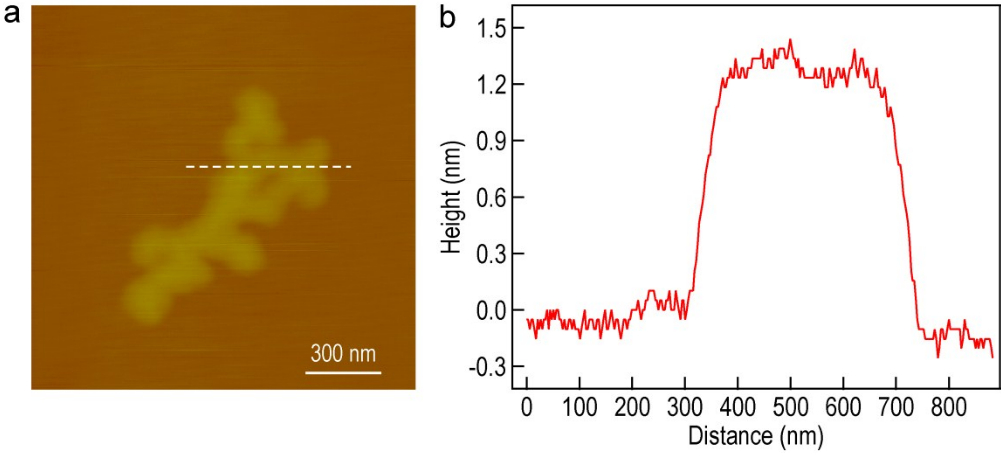

Fig. S1 AFM characterization. (a) AFM image of a representative g-C_3N_4 nanosheet. (b) Height profile taken along the white dashed line in the image shown in (a).

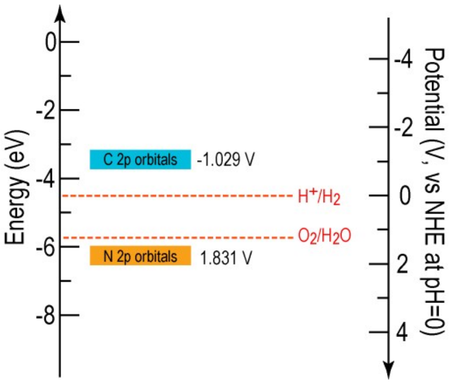

Fig. S2 Band alignment of the g-C_3N_4 nanosheets. It was determined from the optical absorption and electrochemical Mott-Schottky plots.

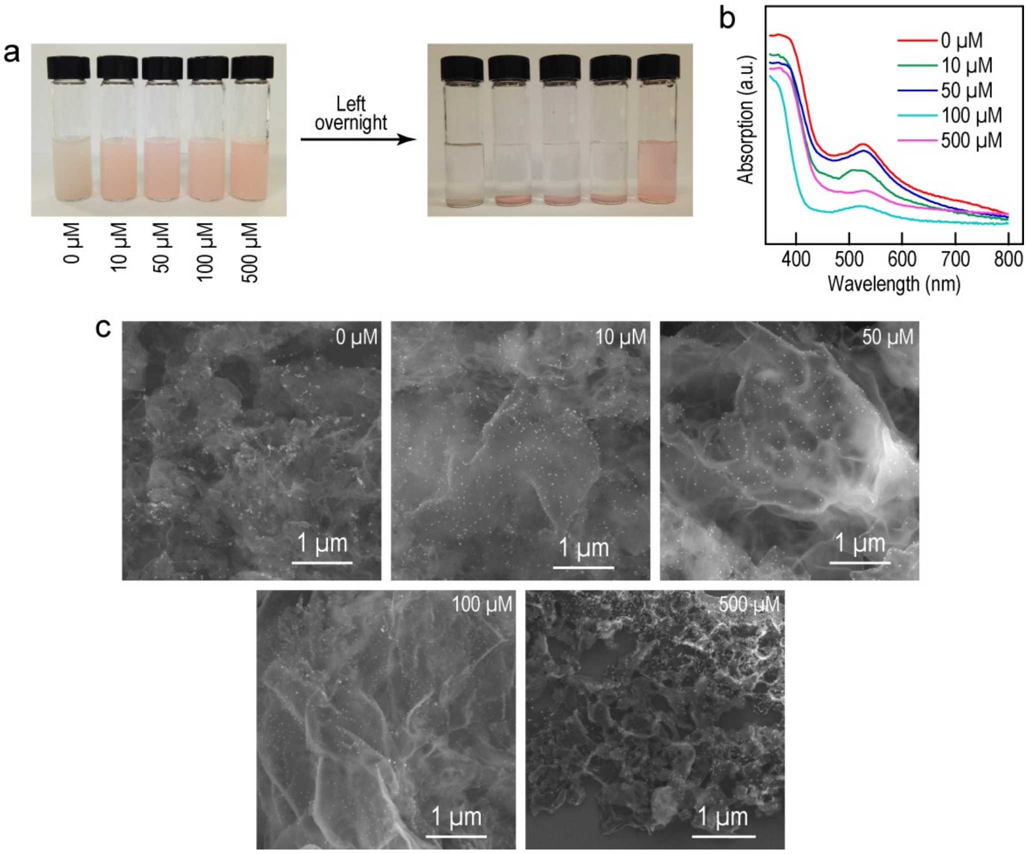

Fig. S3 Effect of the CTAB concentration on the assembly. (a) Photographs of the electrostatic assembly between the 18-nm-sized Au NSs and the g-C_3N_4 nanosheets at different CTAB concentrations. (b) Absorption spectra of the products obtained at different CTAB concentrations. (c) SEM images of the corresponding products. The content of the Au NSs in the assembly process was all adjusted to be 2.0 wt%.

Fig. S3a shows the photographs of the Au NS18/g-C_3N_4 samples prepared at different CTAB concentrations of 0, 10, 50, 100 and 500 μM. After the addition of the desired amount of the

Au NSs into the g-C_3N_4 suspension, the resultant mixture was kept under stirring for 3 h to obtain a homogeneous dispersion and then left overnight. Without CTAB, the precipitate at the bottom of the vial is grey pink, while the color of the precipitate is pink when the CTAB concentration is 10, 50 and 100 μM, respectively. However, when the CTAB concentration is increased to 500 μM, the supernatant is pink, suggesting an incomplete adsorption of the Au NSs on the g-C_3N_4 nanosheets. These observations suggest that if the CTAB concentration is too low, the colloidal Au NSs tend to aggregate on the g-C_3N_4 nanosheets. On the contrary, if the CTAB concentration is too high, excess CTAB molecules will compete with the CTAB-capped Au NSs, leading to the unsuccessful deposition of the Au NSs on the g-C_3N_4 nanosheets. The effect of the CTAB concentration on the assembly of the Au NSs on the g-C_3N_4 nanosheets was confirmed by the absorption spectra and SEM images of the collected samples in Fig. S3b and c. The appropriate CTAB concentration for the assembly of the Au NSs is in the range of 10–100 μM.

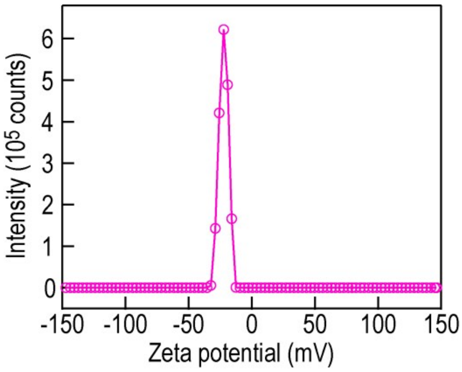

Fig. S4 Zeta potential of the reaction solution for the assembly of Au NS18/g-C_3N_4. The CTAB concentration in the solution is 50 μM.

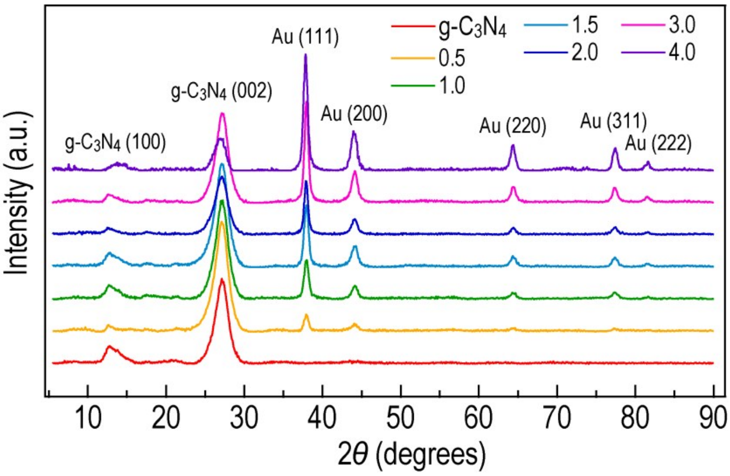

Fig. S5 XRD patterns of the g-C_3N_4 nanosheets and the Au NS18/g-C_3N_4 samples of different Au loading amounts. The diffraction peaks of Au are indexed according to the standard pattern of JCPDS No. 01-1174.

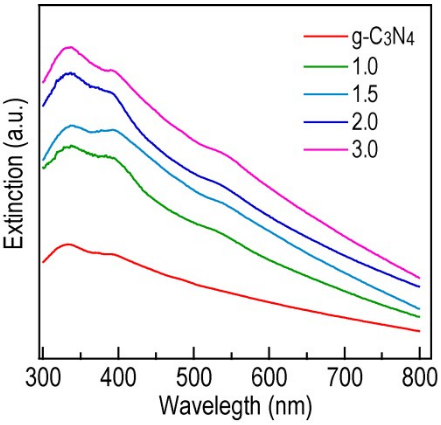

Fig. S6 Extinction spectra of the g-C_3N_4 and Au NS18/g-C_3N_4 samples in aqueous solutions with the Au contents of 1.0, 1.5, 2.0 and 3.0 wt%. The concentrations of the samples are all 0.5 mg mL^{-1}.

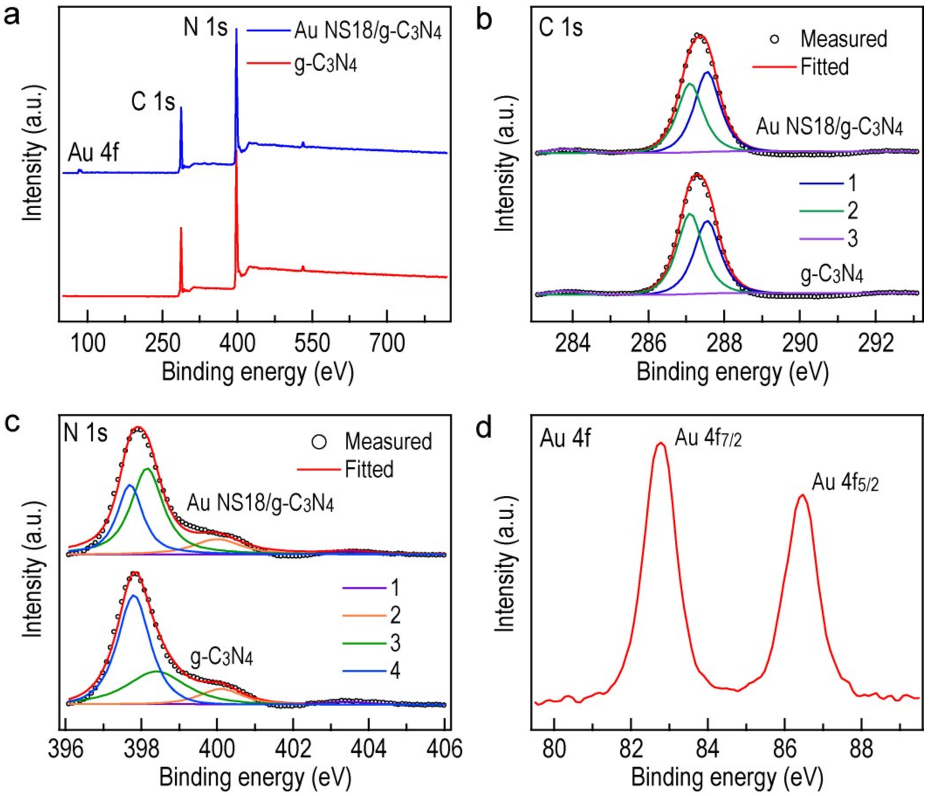

Fig. S7 XPS measurements of the g-C_3N_4 nanosheets and the Au NS18/g-C_3N_4 sample. (a) Survey spectra. (b) C 1s spectra. (c) N 1s spectra. (d) Au 4f spectrum. The Au loading in the hybrid nanostructure sample is 2.0 wt%. The labeled spectra in (b and c) are the fitted peaks.

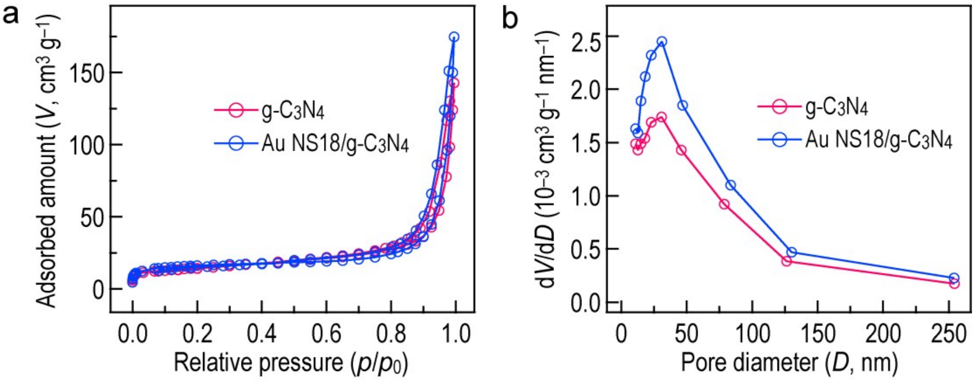

Fig. S8 Nitrogen adsorption-desorption measurements. (a) Adsorption-desorption isotherm curves of the g-C_3N_4 and 2.0 wt% Au NS18/g-C_3N_4 samples. (b) Corresponding pore size distribution curves.

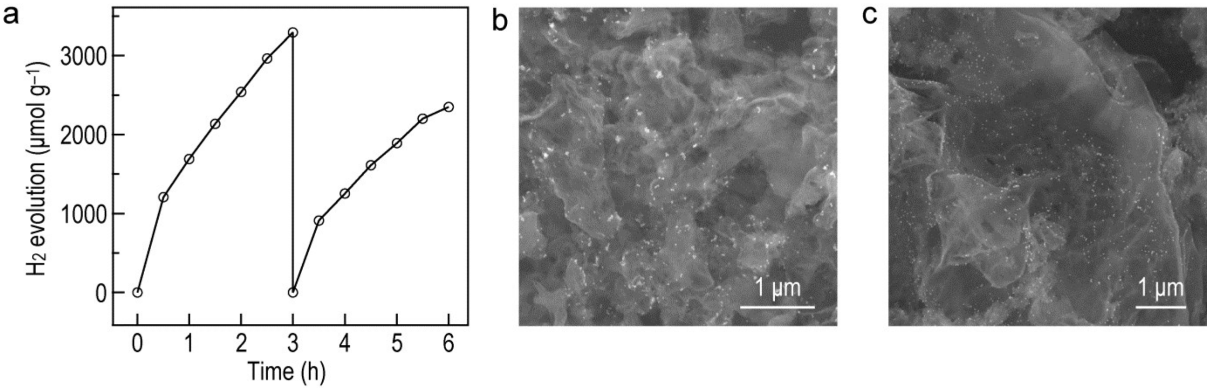

Fig. S9 Effect of CTAB on the photocatalytic stability. (a) H_2 evolution over the 2.0 wt% Au NS18/g-C_3N_4 sample under visible light from water containing 2.5 vol% of TEOA in the absence of CTAB. (b) SEM image of the 2.0 wt% Au NS18/g-C_3N_4 sample after H_2 evolution in the absence of CTAB. (c) SEM image of the 2.0 wt% Au NS18/g-C_3N_4 sample after H_2 evolution in the presence of CTAB.

Fig. S9a shows the photocatalytic H_2 evolution over the 2.0 wt% Au NS18/g-C_3N_4 sample under visible light in the absence of CTAB molecules. In the second cycle, the H_2 generation rate decreases from 1098 to 782 μmol g^{-1} h^{-1}, only 71% of that in the first cycle. We believe that the reduced activity is caused by the competition between TEOA molecules and the g-C_3N_4 nanosheets for the attraction of the CTAB-capped Au NSs. The SEM images of the photocatalysts in Fig. S9b and c after the stability test confirm the speculation. The aggregation of the Au NSs over the g-C_3N_4 nanosheets was observed in the absence of CTAB molecules (Fig. S9b) while there is no sign for the aggregation of the Au NSs after the photocatalytic stability test in the presence of CTAB molecules (Fig. S9c).

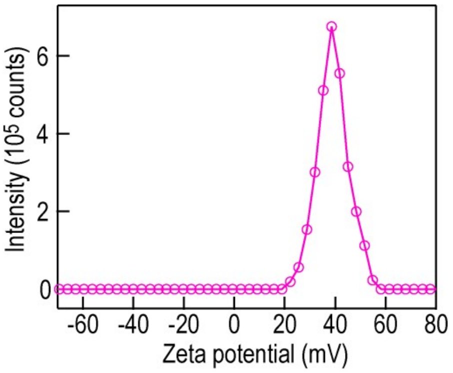

Fig. S10 Zeta potential of the Au NS18/g-C_3N_4 hybrid nanostructure sample in the photocatalytic reaction solution. The CTAB concentration is 18 mM.

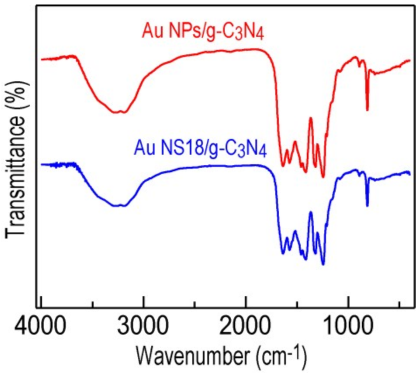

Fig. S11 FTIR spectra of the Au NPs/g-C_3N_4 and Au NS18/g-C_3N_4 samples.

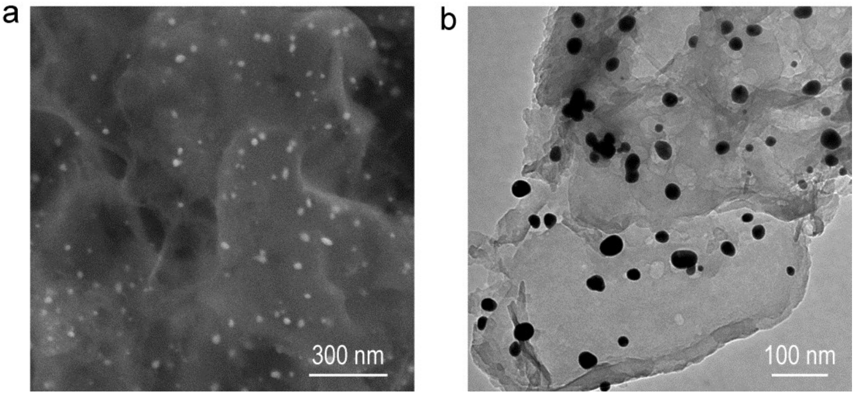

Fig. S12 Photodeposition of Au NPs on the g-C_3N_4 nansheets. (a) SEM image of the Au NPs photodeposited on the g-C_3N_4 nanosheets. (b) TEM image of the corresponding sample.

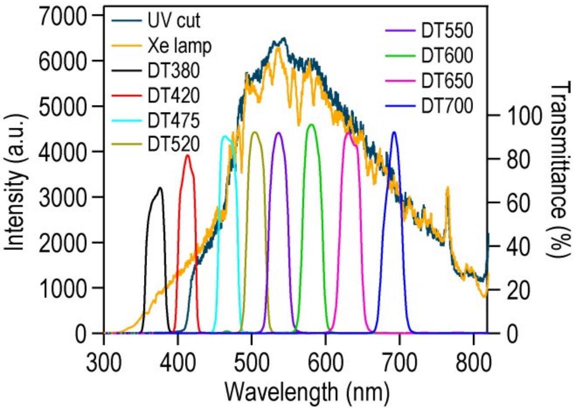

Fig. S13 Emission spectrum of the Xe lamp light source (left axis). The curve labeled with “Xe lamp” represents the full spectrum of the Xe lamp without any filter. The curve labeled with “UV cut” represents the visible light ($\lambda > 420$ nm) that was obtained from the Xe lamp using a 420-nm cut-off filter. The other curves are the transmission spectra of the bandpass filters with different central wavelengths (right axis). These bandpass filters were employed to provide monochromatic light. Their full widths at half maximum are all 20 nm.

Supplementary tables

Table S1 Compositions and pore properties of the g-C_3N_4 nanosheet sample and the 2.0 wt% Au NS18/g-C_3N_4 sample

Sample	C (atomic %)	N (atomic %)	Au (atomic %)	S_{BET} (m^2 g^{-1})	Pore size (nm)
g-C_3N_4	42.01	57.99		50	30.5
Au NS18/g-C_3N_4	41.91	57.95	0.14	59	31.3

Table S2 Comparison of the H_2 evolution rates among reported photocatalysts made of plasmonic Au nanoparticles and g-C_3N_4

Catalyst	Light source	Reaction conditions	H_2 evolution rate (μmol g^{-1} h^{-1})	Reference
Au/g-C_3N_4	300 W Xe lamp, $\lambda >$ 420 nm	Aqueous TEOA solution (2.5 vol%)	540	This work
Au/CN	300 W Xe lamp, $\lambda >$ 420 nm	Aqueous solution containing methanol (20 vol%)	112	1
Au clusters/g-C_3N_4	300 W Xe lamp, $\lambda \geq$ 420 nm	Mixed solution of water and methanol (v/v, 4:1)	230	2
Au/g-C_3N_4	High-pressure 300 W Xe lamp, $\lambda >$ 420 nm	Aqueous TEOA solution (10 vol%)	553	3
Au/g-C_3N_4	$\lambda \geq$ 400 nm	Aqueous TEOA solution (10 vol%)	~550	4
Pt/g-C_3N_4	300 W Xe lamp, $\lambda >$ 420 nm	Aqueous TEOA solution (10 vol%)	73 μmol h^{-1} (the amount of the photocatalyst not mentioned)	5
Au/g-C_3N_4	300 W ultraviolet Xe lamp, $\lambda >$ 420 nm	Aqueous TEOA solution (10 vol%)	94.6	6
Au/g-C_3N_4	125 W medium-pressure visible-light Hg lamp, $\lambda \geq$ 400 nm	Aqueous TEOA solution (10 vol%)	8870	7
$CsTaWO_6$/Au/g-C_3N_4	300 W Xe lamp	Aqueous solution containing methanol (20 vol%)	9.16	8

Au@C_3N_4	300 W Xe lamp, $\lambda >$ 420 nm	Aqueous TEOA solution (6.25 vol%)	~104.2	9
Au/g-CNS	300 W Xe lamp, $\lambda >$ 420 nm	Aqueous solution containing lactic acid (20 vol%)	79	10
Au/g-C_3N_4	150 W Xe lamp, $\lambda >$ 420 nm	0.25 M Na_2S and 0.35 M Na_2SO_3 aqueous solution	~1000	11
Au/g-C_3N_4	300 W Xe lamp, $\lambda >$ 420 nm	Mixture solution of methanol and water (v/v, 3:7)	223	12
Au/g-C_3N_4/TiO_2 nanofibers	300 W Xe lamp, $\lambda >$ 400 nm	Aqueous TEOA solution (15 vol%)	42	13
Au/g-C_3N_4	350 W Xe lamp, $\lambda >$ 400 nm	Aqueous solution containing methanol (25 vol%)	32	14
Au/g-C_3N_4/P25	300 W Xe lamp, $\lambda >$ 420 nm	Mixture solution of methanol and water (v/v, 3:7)	253	15
Au/g-C_3N_4	300 W Xe lamp, $\lambda >$ 420 nm	Aqueous solution containing methanol (17 vol%)	1.25	16

Table S3 Calculated AQY values at different wavelengths[a]

Wavelength (nm)	H_2 evolved (μmol h^{-1})	Light density (mW cm^{-2})	Light power (mW)	AQY (%)
380	3.02	1.13	43.43	1.22
420	3.20	3.45	132.56	0.38
475	0.99	3.69	142.06	0.10
520	1.10	3.69	141.83	0.10
550	0.29	3.63	139.8	0.03
600	0.18	3.79	145.68	0.02
650	0	3.84	147.72	0
700	0	3.66	140.93	0

[a] The diameter of the reactor is 7 cm.

An example is given below for the calculation of the AQY.

λ = 380 nm

The number of incident photons is

$$N_{\text{incident}} = \frac{Pt}{h\nu} = \frac{Pt\lambda}{hc} = \frac{43.43 \times 10^{-3} \times 3600 \times 380 \times 10^{-9}}{6.63 \times 10^{-34} \times 3 \times 10^{8}} = 2.99 \times 10^{20}$$

In the equation above, P is the light power, t is the irradiation time (1 hour = 3600 seconds), h is Planck's constant, v is the light frequency, and c is the speed of light in free space.

The number of reacted electrons is

$$N_{\text{reacted}} = 2 \times \text{the number of evolved } H_2 \text{ molecules} = 2 \times 3.02 \times 10^{-6} \times 6.02 \times 10^{18}$$

The AQY value can then be calculated as

$$AQY = \frac{N_{\text{reacted}}}{N_{\text{incident}}} \times 100\% = \frac{3.64 \times 10^{18}}{2.99 \times 10^{20}} \times 100\% = 1.2\%$$

λ = 520 nm

$$N_{\text{incident}} = \frac{Pt}{h\nu} = \frac{Pt\lambda}{hc} = \frac{141.83 \times 10^{-3} \times 3600 \times 520 \times 10^{-9}}{6.63 \times 10^{-34} \times 3 \times 10^{8}} = 1.33 \times 10^{21}$$

$$N_{\text{reacted}} = 2 \times \text{the number of evolved } H_2 \text{ molecules} = 2 \times 1.10 \times 10^{-6} \times 6.02 \times 10^{18}$$

$$AQY = \frac{N_{\text{reacted}}}{N_{\text{incident}}} \times 100\% = \frac{1.32 \times 10^{18}}{1.33 \times 10^{21}} \times 100\% = 0.1\%$$

Supplementary references

1 A. Zada, M. Humayun, F. Raziq, X. L. Zhang, Y. Qu, L. L. Bai, C. L. Qin, L. G. Jing and H. G. Fu, *Adv. Energy Mater.*, 2016, **6**, 1601190.

2 W. R. Cheng, H. Su, F. M. Tang, W. Che, Y. Y. Huang, X. S. Zheng, T. Yao, J. K. Liu, F. C. Hu, Y. Jiang, Q. H. Liu and S. Q. Wei, *J. Mater. Chem. A*, 2017, **5**, 19649.

3 J. Zeng, T. Song, M. X. Lv, T. T. Wang, J. Y. Qin and H. P. Zeng, *RSC Adv.*, 2016, **6**, 54964.

4 S. Patnaik, S. Martha, G. Madras and K. Parida, *Phys. Chem. Chem. Phys.*, 2016, **18**, 28502.

5 Y. F. Zhang, F. Mao, H. J. Yan, K. W. Liu, H. M. Cao, J. G. Wu and D. Q. Xiao, *J. Mater. Chem. A*, 2015, **3**, 109.

6 C. C. Han, L. E. Wu, L. Ge, Y. J. Li and Z. Zhao, *Carbon*, 2015, **92**, 31.

7 S. Samanta, S. Martha and K. Parida, *ChemCatChem*, 2014, **6**, 1453.

8 J. Y. Lang, M. Q. Liu, Y. G. Su, L. J. Yan and X. J. Wang, *Appl. Surf. Sci.*, 2015, **358**, 252.

9 S. J. Liang, Y. Z. Xia, S. Y. Zhu, S. Zheng, Y. H. He, J. H. Bi, M. H. Liu and L. Wu, *Appl. Surf. Sci.*, 2015, **358**, 304.

10 W. B. Li, C. Feng, S. Y. Dai, J. G. Yue, F. X. Hua and H. Hou, *Appl. Catal. B: Environ.*, 2015, **168–169**, 465.

11 X. M. Ma, Q. T. Jiang, W. M. Guo, M. Zheng, W. C. Xu, F. B. Ma and B. R. Hou, *RSC Adv.*, 2016, **6**, 28263.

12 L. H. Xie, Z. Y. Ai, M. Zhang, R. Z. Sun and W. R. Zhao, *PLoS One*, 2016, **11**, e0161397.

13 X. B. Wei, C. L. Shao, X. H. Li, N. Lu, K. X. Wang, Z. Y. Zhang and Y. C. Liu, *Nanoscale*, 2016, **8**, 11034.

14 J. Jiang, J. G. Yu and S. W. Cao, *J. Colloid Interface Sci.*, 2016, **461**, 56.

15 W. R. Zhao, L. H. Xie, M. Zhang, Z. Y. Ai, H. P. Xi, Y. J. Li, Q. M. Shi and J. S. Chen, *Int. J. Hydrogen Energy*, 2016, **41**, 6277.

16 X. L. Ding, Y. X. Li, J. Zhao, Y. Q. Zhu, Y. Li, W. Y. Deng and C. Y. Wang, *APL Mater.*, 2015, **3**, 104410.